Wind and Structures, Vol. 14, No. 3 (2011) 187-208
DOI: http://dx.doi.org/10.12989/was.2011.14.3.187

Aerodynamic flutter analysis of a new suspension bridge with double main spans

W.M. Zhang[1], Y.J. Ge*[1] and M.L. Levitan[2]

[1]State Key Laboratory for Disaster Reduction in Civil Engineering, Department of Bridge Engineering, Tongji University, Shanghai 200092, P.R.China
[2]Civil and Environmental Engineering Department, Louisiana State University, Baton Rouge, LA 70803, United States

(Received May 13, 2010, Accepted October 11, 2010)

Abstract. Based on the ANSYS, an approach of full-mode aerodynamic flutter analysis for long-span suspension bridges has been presented in this paper, in which the nonlinearities of structure, aerostatic and aerodynamic force due to the deformation under the static wind loading are fully considered. Aerostatic analysis is conducted to predict the equilibrium position of a bridge structure in the beginning, and then flutter analysis of such a deformed bridge structure is performed. A corresponding computer program is developed and used to predict the critical flutter wind velocity and the corresponding flutter frequency of a long-span suspension bridge with double main span. A time-domain analysis of the bridge is also carried out to verify the frequency-domain computational results and the effectiveness of the approach proposed in this paper. Then, the nonlinear effects on aerodynamic behaviors due to aerostatic action are discussed in detail. Finally, the results are compared with those of traditional suspension bridges with single main span. The results show that the aerostatic action has an important influence on the flutter stability of long-span suspension bridges. As for a suspension bridge with double main spans, the flutter mode is the first anti-symmetrical torsional vibration mode, which is also the first torsional vibration mode in natural mode list. Furthermore, a double main-span suspension bridge is better in structural dynamic and aerodynamic performances than a corresponding single main-span structure with the same bridging capacity.

Keywords: suspension bridge; double main spans; full-mode; flutter; aerostatic action.

1. Introduction

As a human dream and an engineering challenge, the structural engineering of bridging larger obstacles has entered into a new era of crossing wide rivers and sea straits, for example, the Yangtze River in China, the Messina Strait in Italy, the Tsugaru Strait in Japan, the Gibraltar Strait linking European and African Continents, and so on. One of the most interesting challenges has been identified as bridging capacity, in particular of suspension bridges as a bridge type with potential longest span. Traditionally, bridging capacity refers to a single bridge span, for example, the Akashi Kaikyo Bridge with a central span of 1991 m. The tendency of bridging capacity

* Corresponding Author, Professor, PhD, E-mail: yaojunge@tongji.edu.cn

development is not only an invention to make the span longer, but also a further or new development of the concept to make continuous multiple main span schemes (Ge *et al*. 2009). Under the rapid development of suspension bridges, China launched two long-span suspension bridges with double main spans longer than 1000 m in 2007. One of them is the Taizhou Bridge across the Yangtze River with the span arrangement of 390+2×1080+390 m, and the other is the Maanshan Bridge over the Yangtze River spanned as 360+2×1080+360 m. Both of these are under construction (Ge and Xiang 2008). Actually, several long-span suspension bridge schemes with continuous double main spans are being planed or designed, such as the Ho-yo Strait Bridge in Japan with a span arrangement of 1100+2×3000+1300 m (Manabu 2008), the Chacao Channel Bridge which will connect the Chiloe Island and the Chile mainland with double main spans of 1055+1100 m, two schemes of the Gibraltar Bridge spanned as 2100+2×4200+2100 m and 1750+2×5000+1750 m, respectively, and so on.

For long-span suspension bridges with double main spans, one of the most important aerodynamic characteristics is flutter instability, which takes place when a bridge is exposed to wind speeds above a certain critical value. At present, several results of wind tunnel tests and research on flutter of traditional suspension bridges with single main span are available, but few studies on flutter instability of suspension bridges with double main spans have been conducted to date. In order to make it convenient for engineers to estimate the flutter performances of suspension bridges with double main spans in preliminary design phase according to those of traditional suspension bridges with single main span, it is necessary to find out the relationship between the critical flutter wind velocities of those two different bridge types. Further investigation is also necessary to determine what the flutter oscillation mode of a suspension bridge with double main spans is, which has become a highly concerned problem.

Flutter analysis is mostly carried out in the frequency domain because of its computational convenience. At present, the multimode approach and the full-mode approach are two general methods for three-dimensional flutter analysis of bridges. Agar (1989), Namini *et al*. (1992), Tanaka *et al*. (1992), Katsuchi *et al*. (1998, 1999) and Ding *et al*. (2002) developed the multimode flutter analysis approach where the system flutter oscillation mode is assumed to be the combination of a few natural modes of the target structure. There are two important questions in the multimode flutter analysis: how to select the natural modes which are expected to be participated in flutter and what is the accuracy of the superposition results. The first question is usually solved by experience, whereas the second one may be proved by some other means such as aeroelastic full model tests. Consequently, the multi-mode flutter analysis is an approximate approach. Moreover, choosing participating modes in the flutter motion beforehand would necessitate much personal participation in the flutter analysis process and reduce its automatic analysis function. Miyata and Yamada (1990), Dung *et al*. (1998), Ge and Tanaka (2000), Ding *et al*. (2002) developed the full-mode flutter analysis approach where the unsteady aerodynamic forces are applied directly to a three-dimensional finite element model of the structure. This approach is accurate in theory because it formulates the asymmetric eigenvalue problem including the entire natural modes and representing all possible system oscillations and gets rid of mode selection and superposition. Hua *et al*. (2007, 2008) incorporated full-mode flutter analysis into the commercial FE package ANSYS utilizing a specific user-defined element *Matrix27*.

In most of the studies mentioned above, the analyses are based on the undeformed initial structures and the nonlinear effects due to the wind-structure interactions are neglected. For long-span suspension bridges, the static wind action will cause the large deformation because of the lower structural stiffness. Large deformation may alter the tangent stiffness and specially the attack angle along the bridge axis therefore, affecting both the mechanical structure and the aerodynamic forces. These effects will consequently influence the aerodynamic stability of the bridge. Katsuchi *et al*. (1998, 1999) and Zhang *et al*. (2002) considered nonlinear effects of aerostatic action in their flutter analysis based on the multimode flutter analysis approach. Dung *et al*. (1998) also took nonlinear effects of aerostatic action into account when the full-mode flutter analysis approach was used, but the mechanics and roles of these effects on the aerodynamic stability of long-span suspension bridges were not clearly clarified.

Based on ANSYS, a full-mode flutter analysis approach considering the nonlinear effects of aerostatic action is presented in this paper. Aerostatic analysis is conducted to predict the equilibrium position of a bridge structure in the beginning, and then flutter analysis of such a deformed bridge structure is performed. A corresponding computer program is developed and used to predict the critical flutter wind velocity and the corresponding flutter frequency of the Maanshan Bridge, which is an aforementioned long-span suspension bridge with double main span. A time-domain analysis of the bridge is also carried out to verify the frequency-domain computational results. Then, the nonlinear effects on aerodynamic behaviors due to aerostatic action are discussed in detail. Finally, the results are compared with those of two traditional suspension bridges with single main span, whose span-lengths are the same as and twice of that of the Maanshan Bridge, respectively.

2. Aerostatic analysis

The aerostatic analysis is to predict the equilibrium position, which is the initial state of bridge oscillation under the dynamic wind action. For the bridge deck, three aerostatic components are applied to the deck, but only the drag component is considered for the cables, hangers and towers. As shown in Fig. 1, the three components of static wind load per unit span applied to the deformed deck are drag force, lift force and pitch moment, which can be expressed in wind axes as

$$\begin{aligned} P_D &= \rho U^2 C_D(\alpha) H/2 \\ P_L &= \rho U^2 C_L(\alpha) B/2 \\ P_M &= \rho U^2 C_M(\alpha) B^2/2 \end{aligned} \tag{1}$$

where P_D, P_L and P_M are drag force, lift force and pitch moment, respectively; ρ is the air density; U is the wind velocity; $C_D(\alpha)$, $C_L(\alpha)$ and $C_M(\alpha)$ are the coefficients of drag force, lift force, and pitch moment in wind axes, respectively; α is the effective attack angle of wind, which is the sum

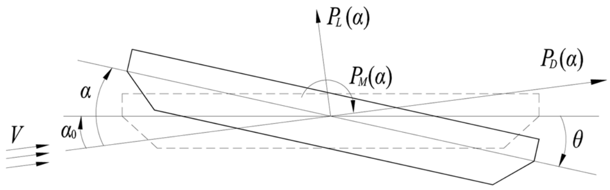

Fig. 1 Three components of static wind load

of the initial attack angle α_0 and the torsional displacement of the deck θ; B is the deck width; H is the vertical projected area of the deck.

The equilibrium equation of the structural system of a bridge under static wind load can be expressed as

$$([K_L(\delta_{j-1})] + [K_{\sigma_{j-1}}(\delta_{j-1})]^{G+W}) \bullet \{\Delta\delta_j\} = \{P_j(U_i, \alpha_j)\} - \{P_{j-1}(U_i, \alpha_{j-1})\} \tag{2}$$

where $[K_L(\delta_{j-1})]$ and $[K_{\sigma_{j-1}}(\delta_{j-1})]^{G+W}$ are, respectively, the structural elastic stiffness matrix and the geometrical stiffness matrix, which are computed using the displacements δ and stresses σ from the preceding iterations; superscripts G and W refer to the gravity and wind loads, respectively; $\{\Delta\delta_j\}$ is the incremental displacement vector; $\{P_j(U_i, \alpha_j)\}$ is the displacement-dependent wind load vector computed using the current effective attack angles of wind; and $\{P_{j-1}(U_i, \alpha_{j-1})\}$ is the displacement-dependent wind load vector computed using the preceding effective attack angles of wind.

The static equilibrium position of bridge structure under a certain wind speed must be solved by the iteration approach because of its double nonlinearity of structure and the static wind force. The procedure of aerostatic analysis can be summarized as follows:

(1) Establish the finite element model of the bridge under investigation, and then determine its initial state under dead load.

(2) Calculate wind load of the structure at a given wind velocity U.

(3) Solve the global equilibrium Eq. (2) for displacement $\{\delta\}$ by the Newton–Raphson method.

(4) Determine the torsional angle of element from the displacement $\{\delta\}$ by averaging the torsional displacement between left node and right node, then calculate effective attack angle of wind and aerostatic coefficients.

(5) Check if the Euclidean norm of aerostatic coefficients is less than the prescribed tolerance. The Euclidean norm is written as

$$\left\{\frac{\sum_{j=1}^{Na}[C_k(\alpha_i) - C_k(\alpha_{i-1})]^2}{\sum_{j=1}^{Na}[C_k(\alpha_{i-1})]^2}\right\}^{1/2} \le \varepsilon_k \tag{3}$$

where N_a is the number of nodes subjected to the displacement-dependent wind load; i is the serial number of current iteration; ε_k is the prescribed tolerance, which can be assumed as 0.005.

(6) If Eq. (2) is not satisfied, repeat steps 2-5. Otherwise, the equilibrium position of the bridge structure has been found, and output the effective wind attack angles of all deck elements.

3. Aerodynamic analysis

When the aerostatic equilibrium position is found, the aerodynamic analysis could be carried out on the deformed bridge structure.

3.1 Aerodynamic force

The aerodynamic force is generally assumed to be composed of: (1) the buffeting force due to turbulence in the oncoming wind flow and (2) the self-excited force due to wind-structure interaction in the smooth oncoming wind flow. The buffeting force usually does not make the bridge aerodynamic unstable, so it is neglected in the aerodynamic analysis. The term self-excited forces describe the forces induced by the motion of the structure, which includes the motion induced by the vortex shedding. Since the vortex-shedding force is usually small in its magnitude compared to the self-excited force related to the flutter instability, it could be ignored in flutter analysis (Ge and Tanaka 2000).

Within the linear aerodynamics, the general expressions for lift force, drag force and pitching moment acting on a moving structure in steady airflow can be represented as follows (Scanlan 1978, Jain *et al.* 1996)

$$L_{se} = \frac{1}{2}\rho U^2(2B)\left(K^2H_4^*\frac{h}{B} + K^2H_6^*\frac{p}{B} + K^2H_3^*\alpha + KH_1^*\frac{\dot{h}}{U} + KH_5^*\frac{\dot{p}}{U} + KH_2^*\frac{B\dot{\alpha}}{U}\right) \tag{4a}$$

$$D_{se} = \frac{1}{2}\rho U^2(2B)\left(K^2P_6^*\frac{h}{B} + K^2P_4^*\frac{p}{B} + K^2P_3^*\alpha + KP_5^*\frac{\dot{h}}{U} + KP_1^*\frac{\dot{p}}{U} + KP_2^*\frac{B\dot{\alpha}}{U}\right) \tag{4b}$$

$$M_{se} = \frac{1}{2}\rho U^2(2B^2)\left(K^2A_4^*\frac{h}{B} + K^2A_6^*\frac{p}{B} + K^2A_3^*\alpha + KA_1^*\frac{\dot{h}}{U} + KA_5^*\frac{\dot{p}}{U} + KA_2^*\frac{B\dot{\alpha}}{U}\right) \tag{4c}$$

where ρ is the air density; U is the mean speed of the oncoming wind; B is the width of the bridge deck; K is the reduced frequency, $K=B\omega/U$; h, p and α are the vertical bending, lateral bending and pitching or torsional displacements, respectively; A_i^*, H_i^* and P_i^*, and (i=1,2,...,6) are all functions of K and experimentally measured flutter derivatives for the deck cross-section under investigation.

Eq. (4) represents the aerodynamic force acting on per unit length of the bridge deck. To convert these uniformly distributed forces into member end effects, a simple lumping procedure is adopted whereby one-half of the force is assumed to act at each member end. Using a space frame element for modeling the overall bridge, the total equivalent aerodynamic joint load, $\{F_{se}\}$, is subdivided into stiffness component $[A_s]$ and damping component $[A_d]$ as

$$\{F_e\} = \frac{1}{2}\rho U^2\left[[A_s]\{q(x,t)\} + \frac{1}{U}[A_d]\{\dot{q}(x,t)\}\right] \tag{5}$$

where $\{q(x,t)\}$, $\{\dot{q}(x,t)\}$ are the displacement and velocity vectors; $[A_s]$, $[A_d]$ are the aerodynamic stiffness and aerodynamic damping matrices.

3.2 Solution of flutter equation

For a structural system, the equation of motion due to the self-excited aerodynamic force can be expressed as

$$[M]\{\ddot{q}(x,t)\} + [D]\{\dot{q}(x,t)\} + [K]\{q(x,t)\} = \frac{1}{2}\rho U^2\left[[A_s]\{q(x,t)\} + \frac{1}{U}[A_d]\{\dot{q}(x,t)\}\right] \tag{6}$$

where $[M]$ is the structural mass matrix; $[D]$ is the structural damping matrix; and $[K]$ is the structural tangent stiffness.

As the aerodynamic stiffness matrices $[A_s]$ and aerodynamic damping matrices $[A_d]$ can be simulated by specific user-defined *Matrix27* elements in ANSYS, the coupled wind-bridge system is first modeled by a hybrid FE model which incorporates structural FE model with *Matrix27* elements used to represent the motion-dependent aeroelastic forces. The stiffness or damping matrices of *Matrix27* element are expressed in terms of wind velocity and vibration frequency. The complex eigenvalues of the low-order modes at varying wind velocities are then determined from this hybrid FE model together with complex eigenvalue analysis, and the real and imaginary parts of the eigenvalues are the logarithm decay rates and damped vibration frequencies of these modes, respectively (Hua *et al*. 2007, 2008). It is appropriate to define the damping ratio of the wind-bridge system as

$$\xi_s = \frac{-\mathrm{Re}(\lambda_t)}{\mathrm{Im}(\lambda_t)} \tag{7}$$

where ξ_s is the damping ratio; λ_t is the eigenvalue of a traced mode; Re and Im are the real and imaginary parts of the complex variable, respectively.

Depending on the sign of the damping ratio, the response can be defined as $\xi_s > 0$, stable; $\xi_s = 0$, neutrally stable; $\xi_s < 0$, unstable. The wind speed that produces the neutrally stable condition is termed as flutter speed.

Bridge flutter is usually bending-torsion coupling divergence or separated flow induced torsional divergence of the deck. Pure vertical or lateral bending vibration divergence of the deck is identified as galloping, which is usually considered to be impossible to occur on cable-supported bridges. For cable-supported bridges, torsional vibration is always involved as a dominant mode in flutter. Therefore, only torsional modes need to be traced in flutter analysis using the approach proposed in the present paper.

3.3 Computational procedure

Based on the above approach, a computational procedure is developed to predict the aerodynamic behaviors under the wind action. The flow of computation can be described as follows:

(1) Establish the initial FE model of the bridge studied, and then determine its initial state under dead load.

(2) Conduct structural mode analysis without damping, and then select a traced mode and get its frequency f_0 and eigenvector.

(3) Assume an initial wind velocity U_0 and a wind velocity increment ΔU.

(4) Under current wind velocity U, perform structural nonlinear aerostatic analysis and obtain the aerostatic equilibrium position.

(5) Establish the FE model of the integrated system with Matrix27 elements, in which the flutter derivatives are inputted through the command TABLE in ANSYS.

(6) Let the system oscillation frequency f_t to be the frequency f_0 of the traced mode, and then determine the reduced wind velocity.

(7) Using the static wind-induced deformation calculated in step 4, the effective wind attack angle between the deck and wind flow can be firstly determined, and then the corresponding flutter derivatives can be calculated by interpolation. Secondly, determine the aeroelastic stiffness and

damping matrices in *Matrix27* elements at the present iteration, and then carry out the damped eigenvalue analysis using the damped solver in ANSYS. It is should be noted that some complex modes including the traced mode may be lost in the damped eigenvalue analysis for bridges with close natural frequencies. This problem can be solved by raising the first shift point for the eigenvalue iterations from zero to a value slightly less than f_0.

(8) Compare the imaginary part of the computed complex eigenvalue λ_t for the traced mode with f_t. If $|(\mathrm{Im}\lambda_t - f_t)/\mathrm{Im}\lambda_t| > 10^{-3}$, let $f_t = \mathrm{Im}\lambda_t$, and repeat steps 7 and 8; otherwise go to step 9. It is to be noted that the order of the traced mode in complex modes computed by the damped eigenvalue analysis may not be the same as that in natural modes. This may cause difficulty for the computer program to find the traced mode automatically without personal participation. Fortunately, mode similarity is helpful to find the traced mode. In all complex modes, the one having maximal mode similarity coefficient with the eigenvector obtained in step 2 is always the traced mode. The mode similarity coefficient can be expressed as

$$C = \frac{(\{v\}^T\{\varphi\})^2}{(\{v\}^T\{v\})(\{\varphi\}^T(\varphi))} \tag{8}$$

where $\{v\}$ and $\{\varphi\}$ are eigenvectors of two modes compared.

(9) If the damping ratio ξ_s for the traced mode is positive, let $U=U+\Delta U$, and repeat steps 4-8; otherwise terminate the iteration.

The lowest critical flutter wind velocity among those of all traced modes chosen from the natural modes and its corresponding frequency are the critical flutter wind velocity and the flutter frequency of the bridge, respectively. As for the wind velocity increment, if it is a small value, too much calculating time is cost; if it is a large value, the critical flutter wind velocity may not be computed accurately. It is suggested that a larger wind velocity increment should be used firstly to find out the wind velocity range which covers the critical flutter wind velocity, followed by detailed analysis with a smaller wind velocity increment in that wind velocity range.

4. Description of the example bridge

The Maanshan suspension bridge over the Yangtze River in Anhui Province of China is used as an engineering example. This bridge with double main spans is spanned as 360 + 2×1080 + 360 m in Fig. 2. All three towers are 176 m high. The height of the middle tower above the deck is 128 m; the height of each side tower above the deck is 143 m symmetrically. The deck cross section (Fig. 3) is an aerodynamically shaped closed box steel deck 38.5 m wide and 3.5 m high. The two cables and all hangers are made of high tensile galvanized parallel wire bundles. The distance between the two cables is 35 m. The spacing between two adjacent hangers is 16.0 m. Section material and geometrical features of main members are indicated in Table 1. The deck is fixed with the middle tower. There are two one-way longitudinal movable supports under the deck on the lower crossbeam of each side tower; lateral wind-resistant supports are set between the deck and the columns of side towers.

As shown in Fig. 4, a three-dimensional finite element model was established for the Maanshan suspension bridge. Three-dimensional beam elements are used to model the three bridge towers. The cables and suspenders are modeled by three-dimensional link elements accounting for geometric nonlinearity due to cable sag. The bridge deck is represented by a single beam and the cross-section

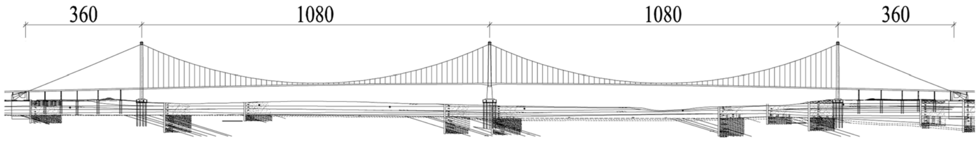

Fig. 2 Elevation of the Maanshan bridge (unit: m)

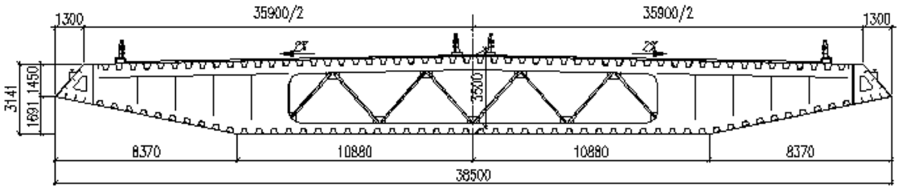

Fig. 3 Cross-section of the deck of the Maanshan bridge (unit: mm)

Table 1 Section geometrical and material features of main members

Main member	J_d (m^4)	I_2(m^4)	I_3(m^4)	I_m(t•m^2/m)	M (t/m)	E (MPa)	γ
Deck	9.10	207.04	3.22	2590	21.39	2.01×10^5	0.3
Cable	-	-	-	-	2.40	2.01×10^5	-
Hanger	-	-	-	-	0.04	2.01×10^5	-

Note: J_d: Torsional moments of inertia; I_2: out-of-plane moments of inertia; I_3: in-plane moments of inertia; I_m: mass moment of inertia per unit length; M: mass per unit length; E: modulus of elasticity; γ: Poisson ratio.

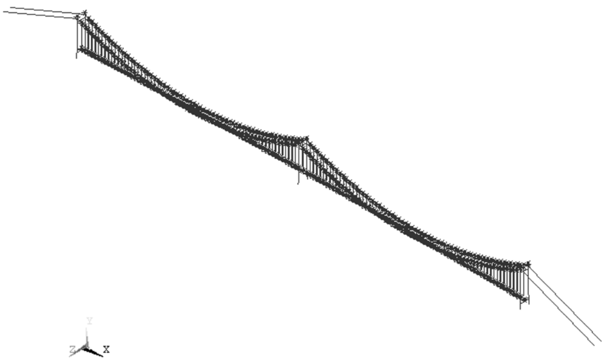

Fig. 4 Finite element model of Maanshan bridge

properties of the bridge deck are assigned to the beam as equivalent properties. The connections between bridge components and the supports of the bridge are properly modeled. Having performed a dynamic finite-element analysis using the Lanczos method in ANSYS, six first-order natural frequencies of various vibration types are extracted in Table 2, and corresponding mode shapes are shown in Fig. 5.

The aerostatic coefficients of the deck are obtained from the sectional model test in wind tunnel as shown in Fig. 6. As shown in Fig. 7, the flutter derivatives under the initial wind attack angles of -3°, -1.5°, 0°, 1.5° and 3° have been experimentally measured from section-model tests in wind tunnel.

Table 2 Natural frequencies of the Maanshan Bridge

Mode	Frequency (Hz)	Mode No.
A-V-1	0.0843	1
S-V-1	0.1169	4
A-L-1	0.0947	2
S-L-1	0.0962	3
A-T-1	0.2675	17
S-T-1	0.3386	26

Note: S-symmetric; A-asymmetric; V-vertical; L-lateral; T-torsional

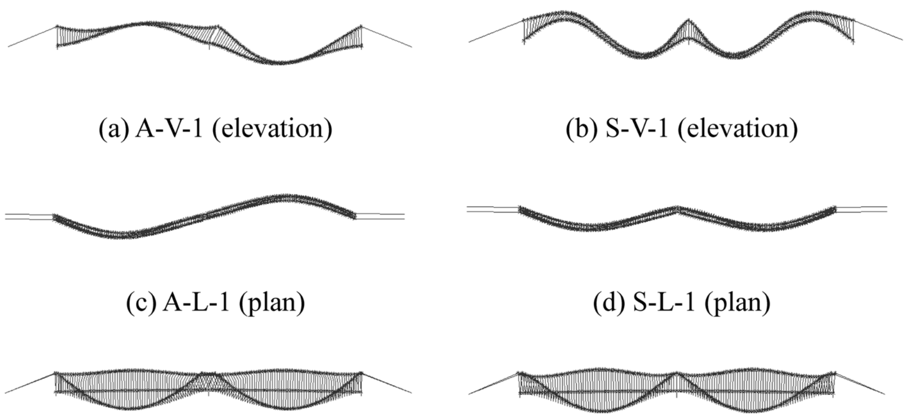

(a) A-V-1 (elevation) (b) S-V-1 (elevation)

(c) A-L-1 (plan) (d) S-L-1 (plan)

(e) A-T-1 (elevation) (f) S-T-1 (elevation)

Fig. 5 Mode shapes of the Maanshan Bridge

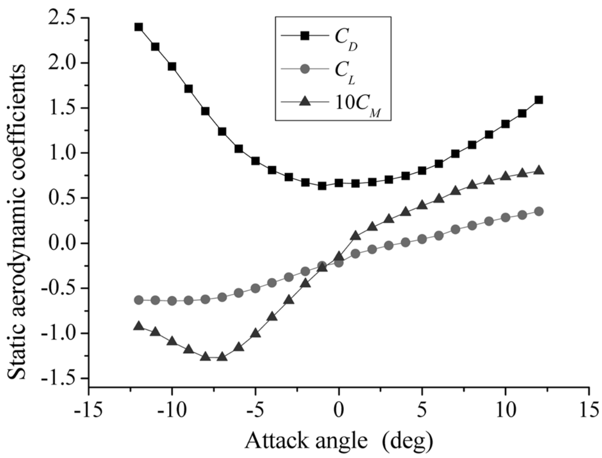

Fig. 6 Aerostatic coefficients of the deck

5. Numerical flutter analysis

5.1 Full-mode analysis

Having assumed structural damping as 0.5%, full-mode flutter analysis under the initial wind attack angles of -3º, 0º and 3º is carried out considering aerostatic action. The A-T-1 and S-T-1 are selected as two traced modes, whose flutter speeds and frequencies are shown in Table 3.

As observed from Table 3, (1) the flutter speed of mode A-T-1 is less than that of mode S-T-1 under any initial attack angle of wind; (2) Initial attack angle of wind has a non-ignorable effect on

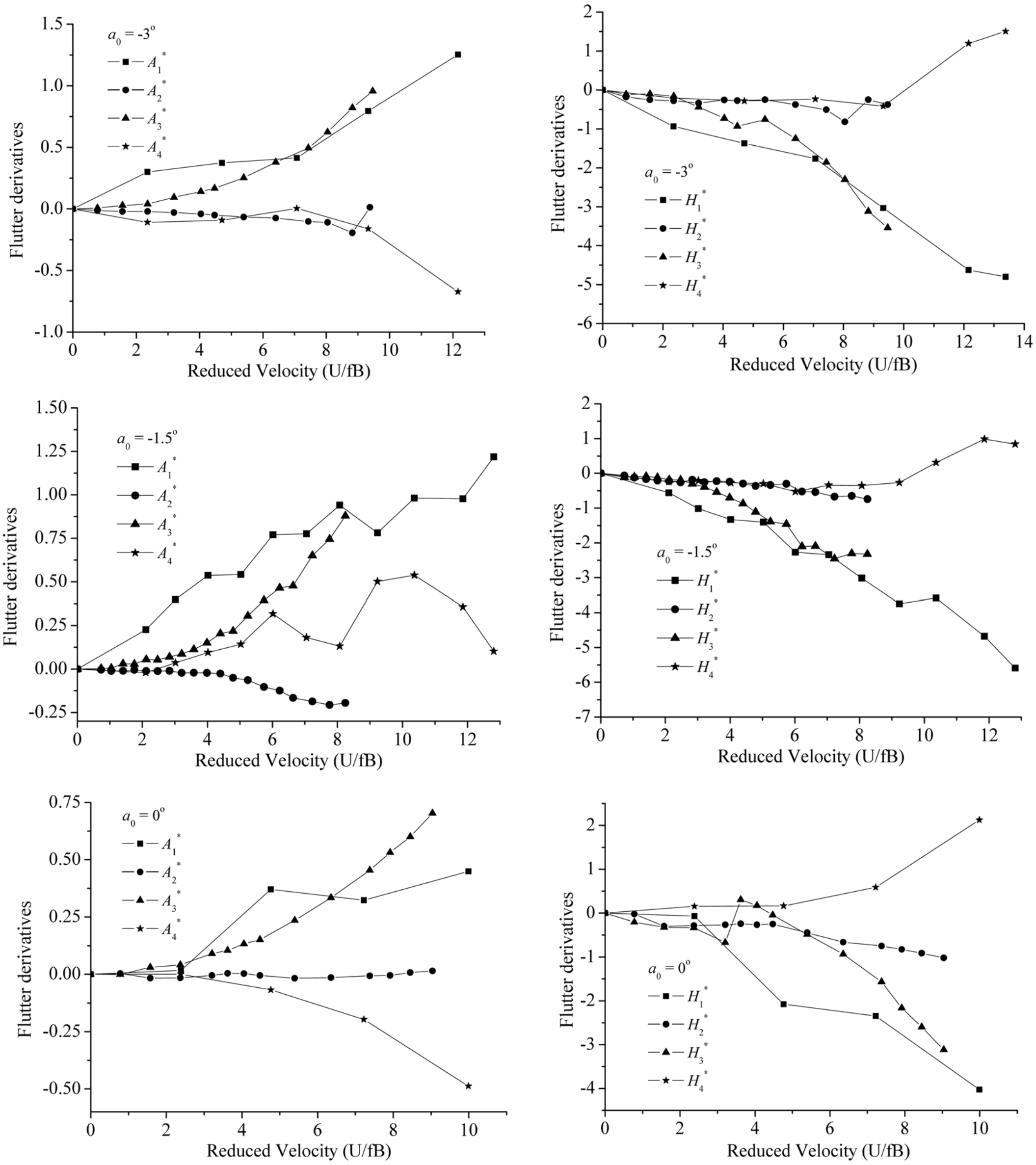

Fig. 7 Flutter derivatives at varying angles of wind incidence versus reduced velocity

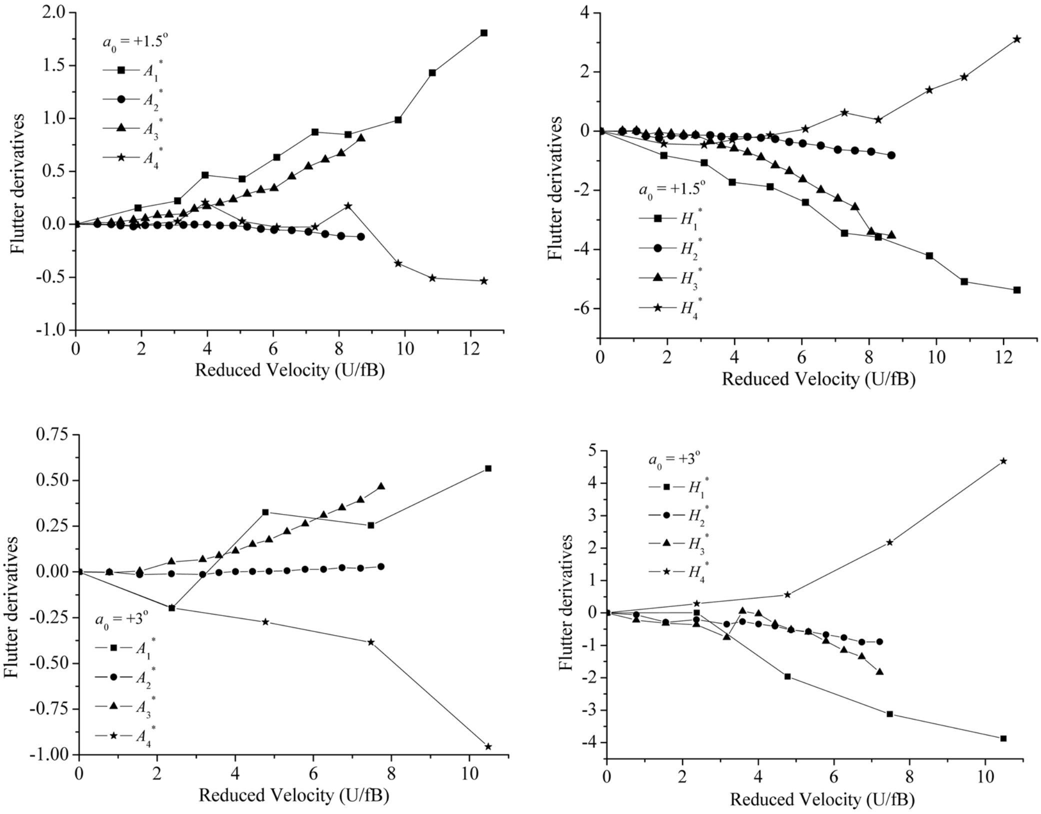

Fig. 7 Continued

Table 3 Flutter analysis results of the Maanshan Bridge

	Initial attack angle	-3°		0°		3°	
	Traced mode	A-T-1	S-T-1	A-T-1	S-T-1	A-T-1	S-T-1
	Flutter frequency (Hz)	0.2506	0.3282	0.2395	0.3002	0.2536	-
Flutter speed (m/s)	Present procedure	89.2	91.0	76.1	94.5	62.5	>98.0
	Section model tests in wind tunnel	81.1	-	76.3	-	70.5	-

flutter speed; (3) The lowest flutter speed is greater than the allowable value 56.6m/s, which means the aerodynamic performance of the Maanshan Bridge is good; (4) A good agreement between the results obtained by the present procedure and wind tunnel tests is observed, especially for the initial attack angle of 0°.

The variations of the damping ratios and frequencies of traced modes under the initial attack angle of 0° versus wind velocity are shown in Figs. 8 and 9, respectively. It is observed that the damping ratio exhibits a significant alteration in the considered wind velocity range, while the frequency decreases slightly with the increase of wind velocity.

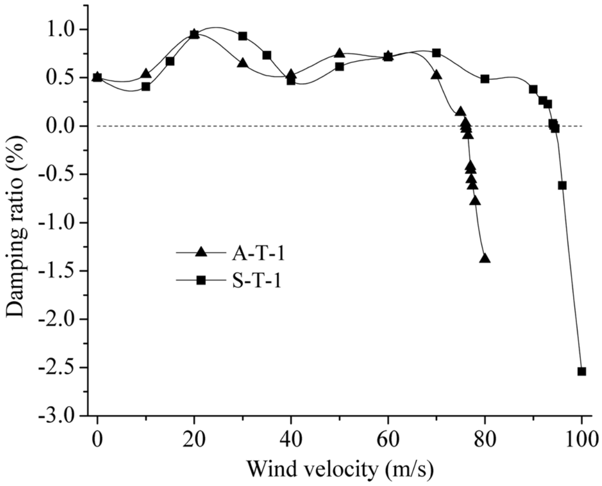

Fig. 8 Variation of damping ratio versus wind velocity

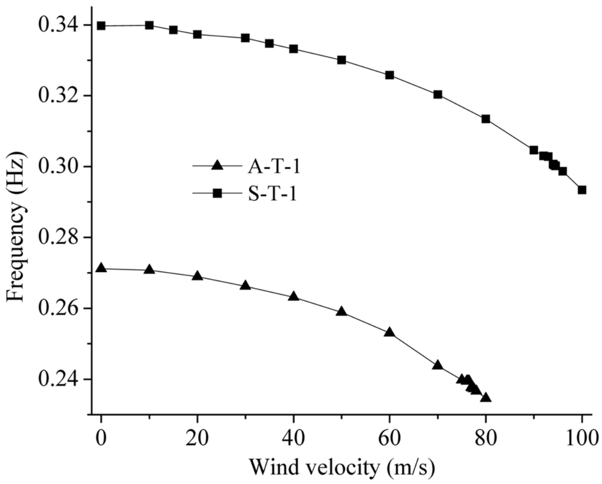

Fig. 9 Variation of frequency versus wind velocity

5.2 Verification by time-domain analysis

In order to verify the above frequency-domain computational results, a time-domain analysis of the integrated system is carried out. For a given wind velocity, the time-domain response of the system subjected to an initial excitation can be readily computed using a time integration scheme. Since the geometric nonlinearity cannot be involved in the above damped eigenvalue analysis, it is not considered in the transient dynamic analysis. Time step size is assumed as 0.05 s, while torsional velocity with a value of 0.01 rad/s is employed as the initial excitation and applied to every node on the deck. However, the torsional velocity for nodes is not available as an initial excitation in the ANSYS, and thus has to be changed into torsional displacement with a value of 0.0005 rad, which is applied to every node on the first time step and then deleted on the second time step.

Under the initial wind attack angle of 0º, the response time histories of each span mid-point for the A-T-1 mode under different wind velocities are obtained by applying anti-symmetrical initial excitations on both spans in the time-domain analysis and shown in Fig. 10. It is recorded that the

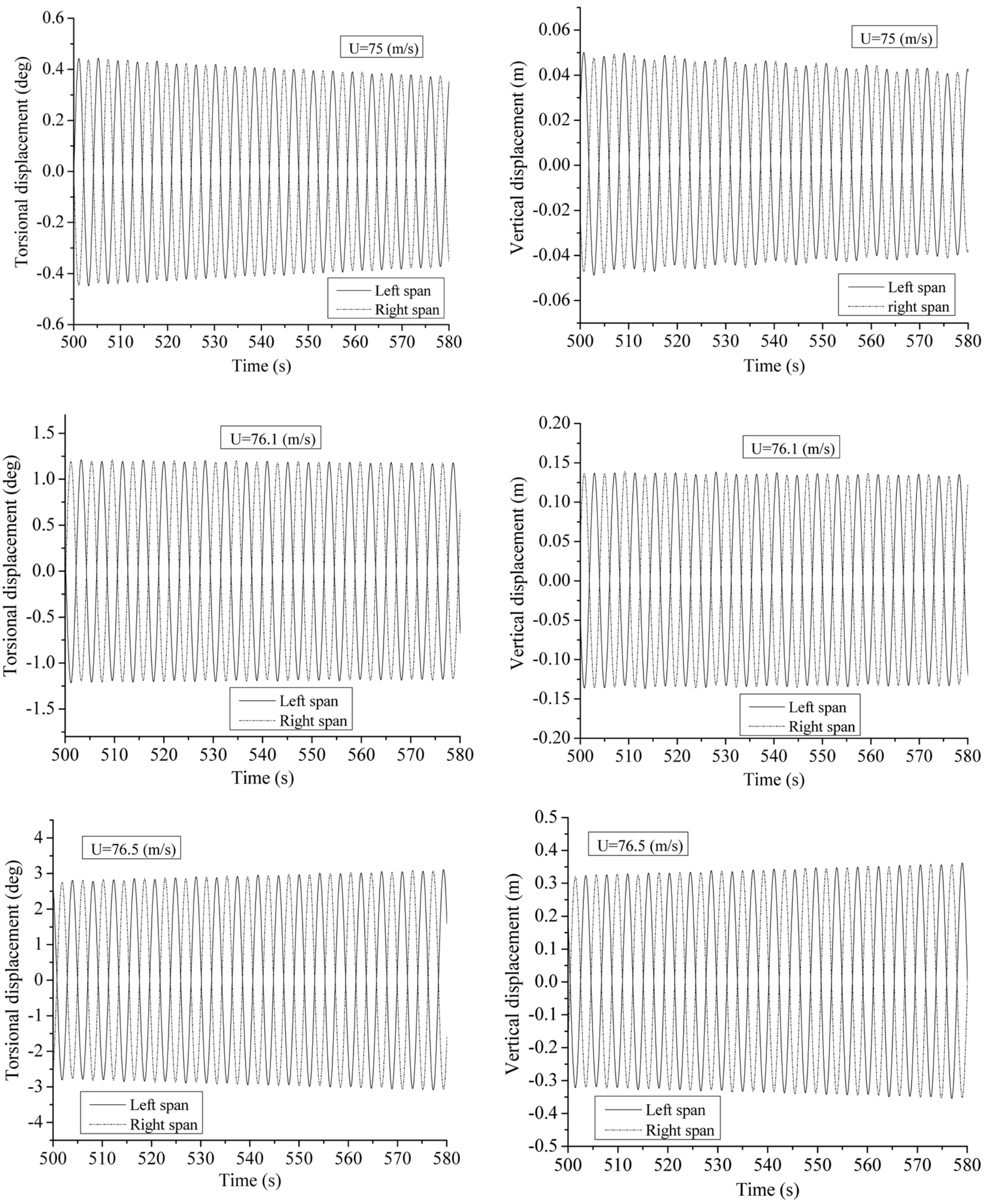

Fig. 10 Time-domain response for the A-T-1 mode

response in the left span and that in the right span are opposite in phase and same in amplitude. By applying symmetrical initial excitations on both spans, the response time histories of each span mid-point for the S-T-1 mode under initial wind attack angle of 0° and different wind velocities are computed in the time-domain analysis. Since the response in the left span is the same as that in the right span, the response time histories of any span mid-point are illustrated in Fig. 11. As Figs. 10 and 11 illustrate, respectively, the system is neutrally stable at the critical wind velocity of 76.1 m/s for the A-T-1 mode and 94.5 m/s for the S-T-1 mode. The system is dynamically stable when the

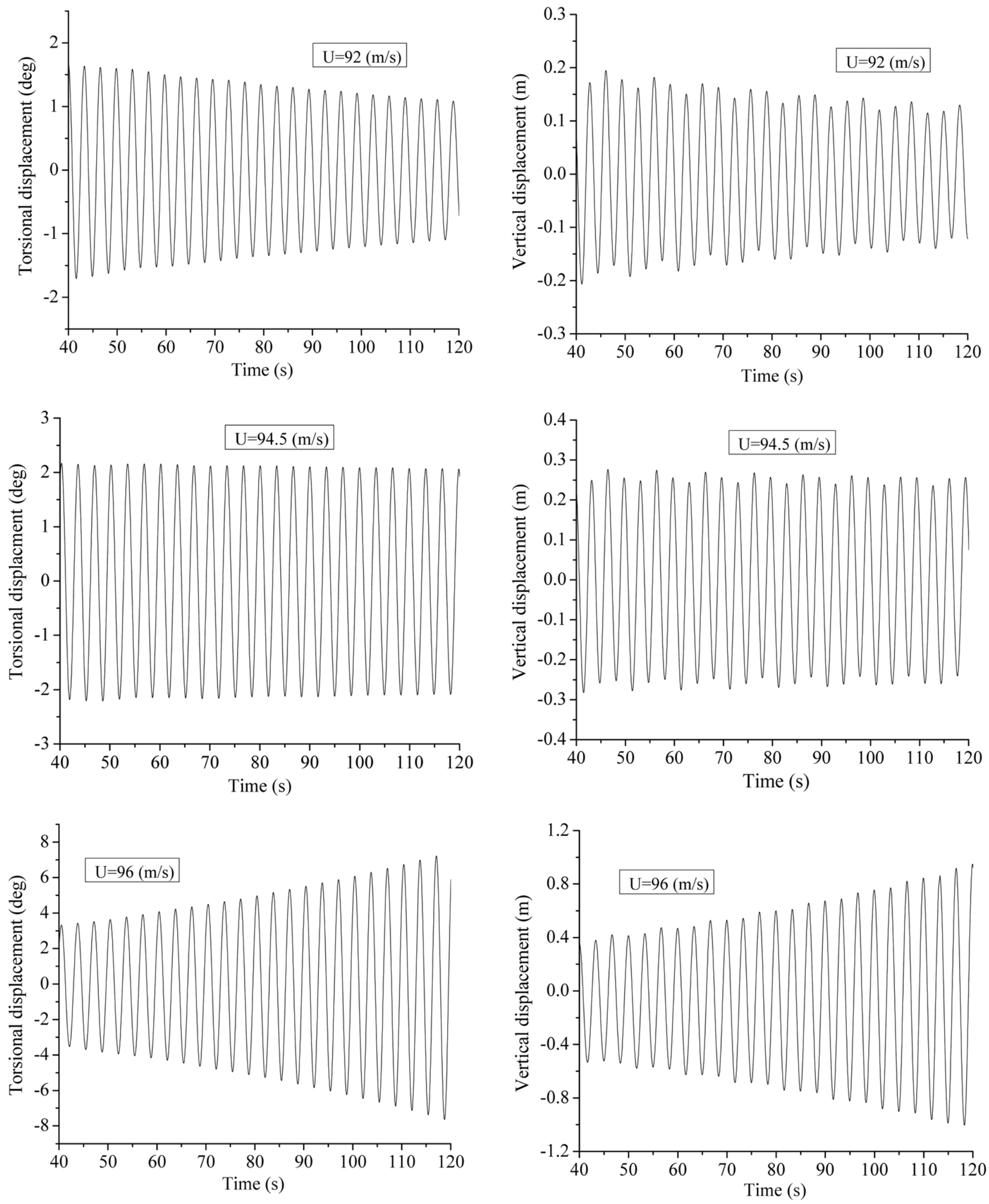

Fig. 11 Time-domain response for the S-T-1 mode

wind velocity is lower than the critical value and becomes dynamically unstable when the wind velocity is greater than the critical value.

5.3 Effect of aerostatic action

Aerostatic action is considered in the above analysis. In order to investigate the effect of the aerostatic action on the flutter stability, full-mode flutter analysis absent of the aerostatic action was carried out, whose results are compared with those of the above analysis in Table 4. It is observed that the aerostatic action has an important influence on the flutter stability of the Maanshan Bridge. Furthermore, the influence degree depends on the initial attack angle of wind and is most remarkable under -3° attack angle, which is mainly due to the additional wind attack angle of the deformed bridge structure under static wind loading. Fig. 12 shows the additional wind attack angles distributing along the bridge deck under the flutter critical condition, in which the additional wind attack angle at -3° attack angle is greater than that at 0° or +3° attack angle.

5.4 Comparison with traditional suspension bridges

In conceptual design point of views, a double main-span suspension bridge is an innovative single main-span structure with an additional supporting pylon at the mid span to improve static and dynamic structural performance. In order to make the comparison of a double main-span suspension bridge and the corresponding single main-span structures, the Maanshan Bridge has been taken as a typical model to create two corresponding comparison models, i.e., Bridge A and Bridge B, which

Table 4 Effect of the aerostatic action on flutter speed

Initial attack angle		-3°		0°		3°	
Traced mode		A-T-1	S-T-1	A-T-1	S-T-1	A-T-1	S-T-1
Flutter speed (m/s)	With aerostatic action	89.2	91.0	76.1	94.5	62.5	>98.0
	Without aerostatic action	78.3	98.3	72.7	92.0	64.4	>97.0
Relative error (%)		12.2	8.0	4.5	2.6	3.0	-

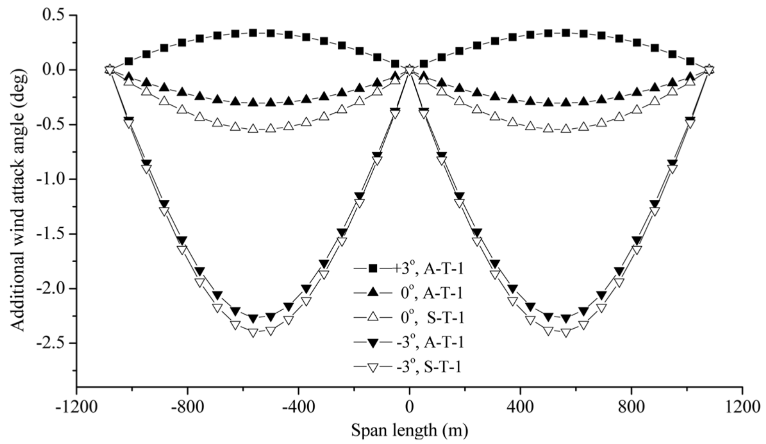

Fig. 12 The additional wind attack angle along the bridge deck at flutter critical condition

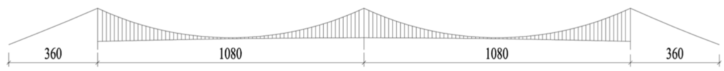

(a) The Maanshan bridge

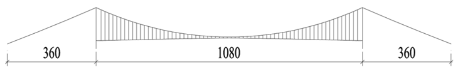

(b) The Bridge A

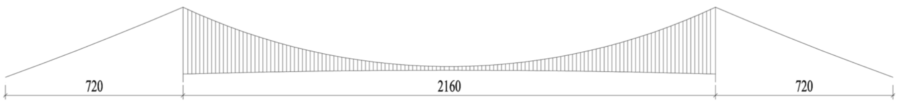

(c) The Bridge B

Fig. 13 Sketches of the Maanshan Bridge and corresponding comparison models

are two traditional single-main-span suspension bridges with the same steel box deck as the Maanshan bridge and spanned as 360+1080+360 m and 720+2160+720 m, respectively, as shown in Fig. 13. It is to be noted that all the structural parameters of the Bridge A are the same as those of the Maanshan Bridge. As for the Bridge B, the rise-span ratio and safety factor of the main cable are the same as those of the Maanshan Bridge due to the taller towers and larger section area of the main cable, respectively.

Having established the FE models for the Bridge A and B, respectively, dynamic analyses were performed, and the first two natural frequencies of the vertical bending, lateral bending and torsional vibration are extracted and compared with those of the Manshan Bridge in Table 5. It is observed that the frequencies of the Bridge A are greater than those of the Manshan Bridge except for the first lateral bending frequency. Moreover, the frequencies of the Maanshan Bridge are significantly enhanced compared with the Bridge B. This is the most important reason why a double main-span suspension bridge is better in structural dynamic performance than a corresponding single main-span structure with the same bridging capacity. In addition, it is interesting to note that the first and second torsional vibration mode of the Bridge A are symmetrical and anti-symmetrical, respectively, while those of the Bridge B are anti-symmetrical and symmetrical, respectively.

Flutter analysis is carried out for the Bridge A and B employing the approach proposed in this paper, and the results under the initial wind attack angles of -3°, 0° and +3° are compared with those of the Maanshan Bridge in Table 6. As can be seen in Table 6, the critical flutter wind velocity of the Maanshan Bridge is greater than those of the Bridge A and B under the initial wind attack angle

Table 5 Natural frequencies of suspension bridges with different span arrangements

Scheme	Span arrangement	Vertical bending (Hz)		Lateral bending (Hz)		Torsional vibration (Hz)	
		First	Second	First	Second	First	Second
Maanshan Bridge	360+2×1080+360m	0.0843	0.1169	0.0947	0.0962	0.2675	0.3386
Bridge A	360+1080+360m	0.1268	0.1470	0.0709	0.2222	0.3218	0.3785
Bridge B	720+2160+720m	0.0829	0.0975	0.0351	0.0744	0.1672	0.1956

Table 6 Critical flutter wind velocities of different bridge schemes

Initial wind attack angle		-3^o	0^o	$+3^o$
Flutter speed (m/s)	Maanshan Bridge	89.2	76.1	62.5
	Bridge A	88.5	90.1	90.0
	Bridge B	55.5	51.0	47.0

of -3^o. However, the Bridge A has the highest critical flutter wind velocity among the three bridges under the initial wind attack angle of 0^o or $+3^o$. It is interesting to find that the Bridge B has the lowest critical flutter wind velocity under any initial wind attack angle due to its longest span and lowest stiffness.

6. Conclusions

Based on the ANSYS, an approach of full-mode aerodynamic flutter analysis for long-span suspension bridges has been presented in this paper, in which the nonlinearities of structure, aerostatic and aerodynamic force due to the deformation under the static wind loading are fully considered. A corresponding program is developed and used to analyze the flutter of a long-span suspension bridge with double main spans. The concluding remarks can be summarized as follows:

(1) The effectiveness of the approach proposed in this paper has been verified by a time-domain analysis.

(2) The flutter mode of a suspension bridge with double main spans is the first anti-symmetrical torsional vibration mode, which is also the first torsional vibration mode in natural mode list.

(3) The initial attack angle of wind has a non-ignorable effect on the flutter speed of a suspension bridge with double main spans.

(4) The aerostatic action has an important influence on the flutter stability of a suspension bridge with double main spans.

(5) A double main-span suspension bridge is better in structural dynamic and aerodynamic performances than a corresponding single main-span structure with the same bridging capacity.

Acknowledgements

The work described in this paper is partially supported by the China Scholarship Council, the NSFC under the Grant 90715039 and the MOST under the Grants 2006AA11Z108 and 2008BAG07B02, which are gratefully acknowledged. The writers also want to thank Mr. Brandon Bass and Ms. Rachel Zimmerman for improving the English of this paper. The valuable comments of the anonymous reviewers of the paper are also acknowledged.

References

Agar, T.J.A. (1989), "Aerodynamic flutter analysis of suspension bridges by a modal technique", *Eng. Struct.*,

11(2), 75-82.
Ding, Q., Chen, A. and Xiang, H. (2002), "Coupled flutter analysis of long-span bridges by multimode and fullorder approaches", *J. Wind Eng. Ind. Aerod.*, **90**(12-15), 1981-1993.
Dung, N. N., Miyata, T., Yamada, H. and Minh, N. N. (1998), "Flutter responses in long span bridges with wind induced displacement by the mode tracing method", *J. Wind Eng. Ind. Aerod.*, **77-78**, 367-379.
Ge, Y. J. and Tanaka, H. (2000), "Aerodynamic analysis of cable-supported bridge by multi-mode and full-mode approaches", *J. Wind Eng. Ind. Aerod.*, **86**(2-3), 123-153.
Ge, Y.J. and Xiang, H.F. (2008), "Bridging Capacity Innovations on Cable-Supported Bridges", *Proceedings of the IABMAS Conference*, Seoul, Korea.
Ge, Y.J., Xu, L.S., Zhang, W.M. and Zhou, Z.Y. (2009), "Dynamic and aerodynamic characteristics of new suspension bridges with double main spans", *Proceedings of the 7th Asia-Pacific Conference on Wind Engineering*, Taipei, Taiwan.
Hua, X.G. and Chen, Z.Q. (2008), "Full-order and multimode flutter analysis using ANSYS", *Finite Elem. Anal. Des.*, **44**(9-10), 537-551.
Hua, X.G., Chen, Z.Q., Ni, Y.Q. and Ko, J.M. (2007), "Flutter analysis of long-span bridges using ANSYS", *Wind Struct.*, **10**(1), 61-82.
Jain, A., Jones, N. P. and Scanlan, R. H. (1996), "Coupled flutter and buffeting analysis of long-span bridges", *J. Struct. Eng-ASCE*, **122**(7), 716-725.
Katsuchi, H., Jones, N. P. and Scanlan, R. H. (1999), "Multimode coupled flutter and buffeting analysis of the Akashi-Kaikyo Bridge", *J. Struct. Eng-ASCE*, **125**(1), 60-70.
Katsuchi, H., Jones, N.P., Scanlan, R.H. and Akiyama, H. (1998), "Multi-mode flutter and buffeting analysis of the Akashi-Kaikyo bridge", *J. Wind Eng. Ind. Aerod.*, **77-78**, 431-441.
Manabu, I. (2008), "21st century super long span bridges in Japan", Documents of China-Japan Workshop on the Technologies of Large Span Bridges, 145-152.
Miyata, T. and Yamada, H. (1990), "Coupled flutter estimate of a suspension bridge", *J. Wind Eng. Ind. Aerod.,* **33**(1-2), 341-348.
Namini, A., Albrecht, P. and Bosch, H. (1992), "Finite element-based flutter analysis of cable-suspended bridges", *J. Struct. Eng-ASCE*, **118**(6), 1509-1526.
Scanlan, R. H. (1978), "Action of flexible bridges under wind, 1: flutter theory", J. Sound Vib., **60**(2), 187-199.
Tanaka, H., Yamamura, N. and Tatsumi, M. (1992), "Coupled mode flutter analysis using flutter derivatives", *J. Wind Eng. Ind. Aerod.*, **42**(1-3), 1279-1290.
Zhang, X.J., Xiang, H.F. and Sun, B.N. (2002), "Nonlinear aerostatic and aerodynamic analysis of long-span suspension bridges considering wind-structure interactions", *J. Wind Eng. Ind. Aerod.,* **90**(9), 1065-1080.

Appendix

(1) Major parts of macro for aerostatic analysis

```
/solu
arad=alfa0*3.1415926/180
:iter
!Apply aerostatic load on girder
*do,i,ngirdmin+1, ngirdmax-1
  Fh=1/2*density*U**2*D*(Cd(i-1,1)*distnd(i-1,i)+Cd(i,1)*distnd(i,i+1))/2
  Fv=1/2*density*U**2*B*(Cl(i-1,1)*distnd(i-1,i)+Cl(i,1)*distnd(i,i+1))/2
  Fz=Fh*cos(arad)-Fv*sin(arad)
  Fy=Fh*sin(arad)+Fv*cos(arad)
  Mt=1/2*density *U**2*B*B*(CM(i-1,1)*distnd(i-1,i)+CM(i,1)*distnd(i,i+1))/2
  f,i,fy,Fy
```

```
   f,i,fz,Fz
   f,i,MX,Mt
*enddo
!Apply aerostatic load on main cables and suspenders
......
!Apply aerostatic load on towers
......
ACEL,0,9.81,0
NLGEOM,1
LNSRCH,1
NROPT,FULL, ,OFF
SSTIF,ON
SOLVE

*do,i,1,ngirdmax
   nrot(i)=rotx(i)
*enddo
*do,i,1,egirdmax
   erot(i)=0.5*(nrot(i)+nrot(i+1))/pi*180
   alfa(i)=alfa0+erot(i)
   Cd(i,1)=coffst(alfa(i), 1)
   Cl(i,1)=coffst(alfa(i), 2)
   CM(i,1)= coffst(alfa(i), 3)
*enddo
! Calculate the Euclidean norm
*set,Cdsumnume,0
*set,Cdsumdeno,0
*set,Clsumnume,0
*set,Clsumdeno,0
*set,CMsumnume,0
*set,CMsumdeno,0
*do,i,1,egirdmax
   Cdsumnume=Cdsumnume+(Cd(i,1)-Cd(i,2))**2
   Cdsumdeno=Cdsumdeno+Cd(i,2)**2
   Clsumnume=Clsumnume+(Cl(i,1)-Cl(i,2))**2
   Clsumdeno=Clsumdeno+Cl(i,2)**2
   CMsumnume=CMsumnume+(CM(i,1)-CM(i,2))**2
   CMsumdeno=CMsumdeno+CM(i,2)**2
*enddo
CdEuClid=sqrt(Cdsumnume/Cdsumdeno)
ClEuClid=sqrt(Clsumnume/Clsumdeno)
CMEuclid=sqrt(CMsumnume/CMsumdeno)
t1=0
t2=0
t3=0
```

```
*if,CdEuclid,le,eps,then ! eps is the prescribed tolerance
  t1=1
*endif
*if,ClEuclid,le,eps,then
  t2=1
*endif
*if,CMEuClid,le,eps,then
  t3=1
*endif
tt=t1+t2+t3
*if,tt,ne,3,then
  *do,i,1,egirdmax
    Cd(i,2)=Cd(i,1)
    Cl(i,2)=Cl(i,1)
    CM(i,2)=CM(i,1)
  *enddo
*endif
*if,tt,ne,3,:iter
```

(2) Major parts of macro for full-mode flutter analysis

```
! Establish the FE model of the integrated system with Matrix27 elements
*do,i,ngirdmin+1,ngirdmax-1
  R,10000+i
  R,20000+i
  n,10000+i,nx(i),ny(i)-3,nz(i)
  TYPE,11
  MAT,11
  REAL,10000+i
  en,10000+i,i,10000+i
  TYPE,12
  MAT,11
  REAL,20000+i
  en,20000+i,i,10000+i
  D,10000+i,all
*enddo

*do,i,ngirdmin+1,ngirdmax-1
  *GET, LENELE1, ELEM,i-1, LENG, , ,
  *GET, LENELE2, ELEM,i, LENG, , ,
  LENELE=(LENELE1+LENELE2)/2
  *GET, RSTIFF, ELEM,10000+i, ATTR, REAL,
  RMODIF,RSTIFF, 13,-density*U*U*(2*pi/UfB)**2*LENELE*H4(i,1)
  RMODIF,RSTIFF, 15,-density*U*U*(2*pi/UfB)**2*LENELE*B*H3(i,1)
  RMODIF,RSTIFF, 83,-density*U*U*(2*pi/UfB)**2*LENELE*B*A4(i,1)
  RMODIF,RSTIFF, 34,-density*U*U*(2*pi/UfB)**2*LENELE*B*B*A3(i,1)
```

```
   *GET, RDAMP, ELEM,20000+i, ATTR, REAL,
   RMODIF,RDAMP, 13,-density*U*B*(2*pi/UfB)*LENELE*H1(i,1)
   RMODIF,RDAMP, 15,-density*U*B*(2*pi/UfB)*LENELE*B*H2(i,1)
   RMODIF,RDAMP, 83,-density*U*B*(2*pi/UfB)*LENELE*B*A1(i,1)
   RMODIF,RDAMP, 34,-density*U*B*(2*pi/UfB)*LENELE*B*B*A2(i,1)
*enddo

!The damped eigenvalue analysis
/SOLU
ANTYPE,2
MSAVE,0
upcoord,1.0,on
ALPHAD,ALPHA
BETAD,BETA
MODOPT,DAMP,100,FREQB,,,off ! FREQB is the first shift point for the eigenvalue iteration
EQSLV,SPAR
MXPAND,100, , ,0
LUMPM,0
PSTRES,1
psolve,triang
PSOLVE,EIGDAMP
expass,on
PSOLVE,EIGEXP
Finish
```

(3) Major parts of macro for time-domain flutter analysis

```
! Establish the FE model of the integrated system with Matrix27 elements
……
! Time-domain flutter analysis
/SOLU
ntime=20000
dtime=0.05
ANTYPE,TRANS
TRNOPT,FULL
acel,,9.81,,
TIMINT,on
NLGEOM,off
PSTRES,1
SSTIF,ON
LUMPM,off
ALPHAD,ALPHA
BETAD,BETA
KBC,1
autots,on
OUTRES,ERASE
```

```
OUTRES,BASIC,LAST,

*do,i,1,1
   nsel,,,,ngirdmin+1,ngirdmax-1
   D,all,rotx,0.0005
   allsel,all
   time,i*dtime
   solve
*enddo

*do,i,2,2
   nsel,,,,ngirdmin+1,ngirdmax-1
   DDEL,all,rotx
   allsel,all
   time,i*dtime
   solve
*enddo

*do,i,3,ntime
   time,i*dtime
   solve
*enddo
finish
```

CC